How Do Crystals Melt?

Simon R. Phillpot, Sidney Yip and Dieter Wolf

Citation: Computers in Physics **3**, 20 (1989); doi: 10.1063/1.4822877
View online: https://doi.org/10.1063/1.4822877
View Table of Contents: https://aip.scitation.org/toc/cip/3/6
Published by the American Institute of Physics

How Do Crystals Melt?

Simon R. Phillpot, Sidney Yip and Dieter Wolf

Computer simulations demonstrate the interplay between thermodynamics and kinetics during the melting process

Melting, the fundamental process in which, at a certain temperature T_m, a crystalline substance undergoes a phase change from a solid to a liquid (melt), still holds mysteries despite its common occurrence. One reason is that in experiments it is still not feasible to observe directly the atomistic details of the process. This means that we do not know the structural arrangements of the atoms or their characteristic motions prior to and during melting—information which is needed in formulating a fundamental theory of the transition. Another reason is that most theoretical methods, including atomic-level computer simulations, do not take into account the effects of extrinsic lattice defects, such as surfaces, dislocations and grain boundaries. The role of lattice defects in the onset of the destruction of long-range order has, consequently, not been clearly established.

Our inability to see *how* melting occurs does not prevent us from knowing *why* it occurs and *when* the order-disorder transition should take place. According to thermodynamics, the melting point T_m is that temperature at which the solid and liquid phases can coexist in equilibrium, a condition which occurs when the Gibbs free energies of the two phases are equal. It is implied that at temperatures above this coexistence temperature the crystal is unstable. However, thermodynamics says nothing about what the *mechanism* of melting is, nor *how long* the process will take. These questions are related to the kinetics of the phenomenon. For a more complete understanding of melting one therefore needs to be concerned with both thermodynamics and kinetics.

Theories of Melting

In a general discussion of melting, one should distinguish from the outset between intrinsic and extrinsic lattice defects. Intrinsic defects, such as lattice vacancies, are produced thermally. By contrast, due to the increase in free energy associated with their creation, extrinsic defects are usually thermodynamically metastable. For example, grain boundaries can be eliminated from polycrystals by high-temperature annealing, thus allowing the material to achieve a state of lower free energy during the process of recrystallization. A number of theories of melting have been proposed during the past seventy years or so, all of which consider only the effects of intrinsic defects. These theories generally assume the dominant mechanism to be one of three types:

(a) According to Lindemann, melting is caused by the onset of an instability when the displacements during thermal vibration of the atoms exceed a certain threshold value ("Lindemann criterion").

(b) According to Born, melting arises from the onset of a mechanical instability, manifesting itself in an imaginary phonon frequency at the onset of which the crystal lattice collapses ("Born instability").

(c) In the theories of Cahn and others, the spontaneous production of intrinsic lattice defects, such as vacancies and intrinsic arrays of dislocations near the

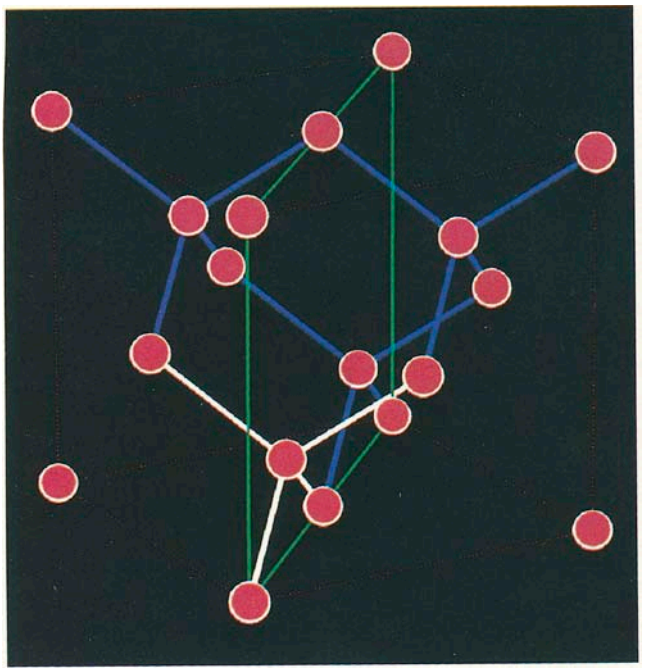

Fig.1: Crystallographic unit cell of the diamond lattice, with silicon atoms denoted by red balls and nearest-neighbor bonds signified in blue. The bonds of one of the four-fold coordinated silicon atoms are highlighted in white. The green rectangle illustrates a (110) plane. The edge of this cubic unit cell defines the lattice parameter, $a = 5.431\text{Å}$, of Si. (1 Angstrom $= 10^{-10}$ m.)

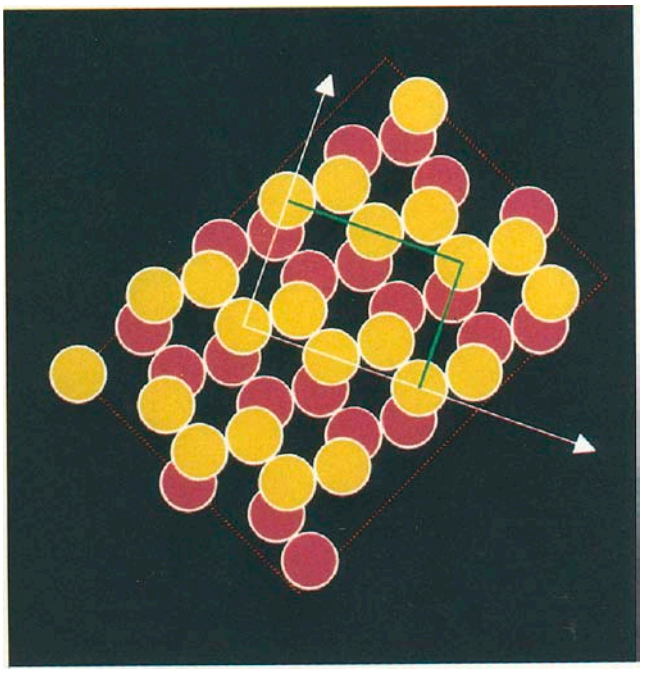

Fig.2: View of the computational cell from above showing the top two (110) planes each containing 22 Si atoms as yellow and red balls, respectively. The dotted gold line encloses the computational cell, which is rotated by 25.24° relative to the <110> and <100> directions in the crystal; the latter are indicated by white arrows. The smaller area enclosed by the green and white lines corresponds to the fraction contained in the single cubic unit cell shown in Fig. 1.

melting point, is thought to be responsible for the breakdown of long-range crystalline order.

These theories have in common that melting is considered as a process occurring *homogeneously* throughout the crystal, with the effects of surfaces, both internal or external, being entirely neglected.

Experimentally, however, it is well known that melting generally proceeds from surfaces into the interior crystalline regions—a process requiring a finite amount of time. For example, about 30 years ago Turnbull and coworkers demonstrated that melting of silica, SiO_2, and phosphorous pentoxide, P_2O_5, are not homogeneous processes but that, instead, the liquid phase nucleates at free surfaces and grain boundaries, from which it propagates into the crystal. Also, recent laboratory experiments by Daeges, Gleiter and Perepezko have demonstrated that small single crystals of silver can be superheated above the melting temperature when coated with gold (which has an almost identical lattice parameter but a higher melting point). Such a coating replaces the silver free surface with a silver-gold interface. Because the lattice parameters of the materials are so similar, however, the effects of such an interface should be small. It was found that the coated pellets could be heated well past the melting point of silver whereas normally, superheating above T_m is known to be difficult to achieve in metals.

These observations not only raise the question of whether melting can, indeed, be regarded as a homogeneous process, but also point to the need for a direct simulational study of melting where surface effects can be isolated, and analyzed in terms of thermodynamics and kinetics.

Molecular-Dynamics Simulation of Silicon at High Temperature

Atomistic modeling, in the form of molecular-dynamics (MD) and Monte Carlo simulations, is a method of studying the cooperative and individual behavior of a system of atoms under well-prescribed conditions. Through the use of interatomic interaction potentials and border conditions, simulations can be made to represent the physical state of a material at finite temperatures and pressures reasonably well. The results of such simulations are particularly valuable for the study of the relation between the atomic structure of a system and its thermodynamic, mechanical, and transport properties. Because of these features, atomistic simulation is increasingly gaining recognition as a means of probing complex physical processes at the atomic level.

The choice of silicon for our simulation of the melting process is motivated by three factors. First, due to its covalent nature of bonding, the crystal structure of silicon is that of cubic diamond, with only four nearest neighbors. Every Si atom may thus be considered to occupy the

center of a tetrahedron, with the four nearest neighbors at the corners (see Fig.1). Upon melting, the tetrahedral coordination is destroyed in favor of an average six-fold coordination in the liquid. By monitoring the average number of nearest neighbors of every atom during the simulation, the four-coordinated "crystalline" Si atoms may readily be distinguished from the six-coordinated "liquid" Si atoms. The fact that a good empirical interatomic potential is available for silicon (derived by Stillinger and Weber) which has been shown to give a rather realistic overall description of its physical properties, provides another reason for our choice of silicon. Finally, silicon is a good choice because extensive experimental data exists on its melting and freezing behavior, including the well-known fact that, like ice, silicon *contracts* upon melting.

In any study of melting, knowledge of the thermodynamic melting point, T_m, is of primary importance. Although any interatomic potential function permits only an approximate description of a given material, it is essential to precisely determine T_m. Using MD methods to determine the temperature-dependent free energies for the crystalline and liquid phases, Broughton and Li obtained a value of $T_m = 1691 \pm 20$K for the Stillinger-Weber potential. That this value is quite close to the known melting point of silicon (1683K) indicates that both the Stillinger-Weber potential function and the molecular-dynamics approach are valid for the study of melting.

A typical molecular-dynamics simulation cell contains several hundred or a few thousand atoms, at most. The basic information that one obtains from such simulations includes, most importantly, the positions and velocities of all the atoms in the system at any instant during the simulation. These variables are obtained by numerically solving Newton's equations of motion for a system of many interacting atoms. Within the limitations of any simulation (pertaining to the approximate nature of the interatomic potential used, and the finite system size and duration of the simulation), the atom positions are like the recorded output of a hypothetical atomic camera, operating with a field of view spanning a distance of no more than about 100 Å at a speed of 10^{14} to 10^{15} frames per second. On such microscopic scales, one can locate unambiguously the position of each atom and follow its motion as it interacts with its neighbors. In the case of silicon we have chosen a time interval of 1.15×10^{-15}s over which Newton's equations of motion are integrated in each time step of the simulation. With lattice-vibration frequencies of typically about 10^{13}s^{-1} for Si, a simulation interval of 1000 time steps (= 1.15 ps) covers approximately 10 vibration periods of each atom.

The purpose of our simulations is to isolate the effects of surfaces and interfaces, and to elucidate the kinetics of the melting process. To investigate the roles played by internal and external surfaces, we have carried out a series of molecular-dynamics simulations of the melting of crystalline silicon, with and without such extrinsic defects, at elevated temperatures. Three model geometries will be considered; the first two focus on the role of grain boundaries and free surfaces, while in the third we investigate the melting behavior of a defect-free perfect crystal. The simulation-cell dimensions, including the number of simulated atoms in the cell, will be chosen to be the same in all three situations, thus eliminating any effects which might possibly arise from different dimensions of the simulation cell as well as numbers of atoms in the cell.

We first investigate the effect of the grain boundary, followed by a simulation of the free (110) surface, in the onset of melting. The planar arrangement of atoms in the rectangular unit cell on the (110) plane is illustrated in Figs.1 and 2. As far as the simulation of melting is concerned, this choice of (110) planes has the advantage that their interplanar spacing, $d(110) = 0.354a$, is much larger than the vibrational amplitudes of the atoms, which are typically no more than about 10% of the nearest-neighbor distance of 0.433a even at the highest temperatures. Here, a is the lattice parameter defined in Fig.1.

Order Parameter for the Melting Transition

Before discussing our simulation results, an order parameter, representing a quantitative measure for characterizing the crystalline and melted regions, has to be defined. If melting were to begin at the surfaces or grain boundaries, then in order to distinguish crystalline from melted regions, it would appear natural, for the purpose of analysis, to subdivide the computational cell into a finite number of slices parallel to the surface or grain boundary and to define some order parameter, ξ, which characterizes quantitatively the degree of crystallinity within each slice. As is common in the area of phase transformations, ξ should be defined such that it varies within the bounds $0 \leqslant \xi \leqslant 1$.

The static structure factor, $S(\mathbf{k})$, is essentially the Fourier transform of the distribution of bond lengths, and may be considered as an order parameter of the crystalline-to-liquid phase transition. From x-ray structure determinations, $S(\mathbf{k})$ is well known to characterize the long-range order in the direction of any vector, $\mathbf{k}$, which is a vector of the reciprocal space lattice. The vectors of this lattice are related to the position vectors, $\mathbf{r}_i$, of the atoms in the real-space lattice by the familiar Ewald relationship:

$$(\mathbf{k}\cdot\mathbf{r}_i) = 2\pi \qquad (1)$$

Being a complex function, with a real and an imaginary part, $S(\mathbf{k})$ directly does not satisfy the requirements imposed on the order parameter ξ. However, its square, given by

$$[S(\mathbf{k})]^2 = |S(\mathbf{k})|^2 = [1/N \Sigma_i \cos(\mathbf{k}\cdot\mathbf{r}_i)]^2 + [1/N \Sigma_i \sin(\mathbf{k}\cdot\mathbf{r}_i)]^2, \qquad (2)$$

varies between zero and one, depending on the values of $(\mathbf{k}\cdot\mathbf{r}_i)$ which range between zero and 2π. We note that the summation in Eq.(2) includes all atoms i in the crystal, with $\mathbf{k}$ being some arbitrary vector. One readily sees that if $\mathbf{k}$ is, indeed, a reciprocal-lattice vector, satisfying Eq.(1), then Eq. (2) yields $[S(\mathbf{k})]^2 \equiv 1$. Since we are interested in the *planar* long-range order parallel to the (110) planes (rather than the *overall* static structure in Eq. (2)), we define a *planar* static structure factor,

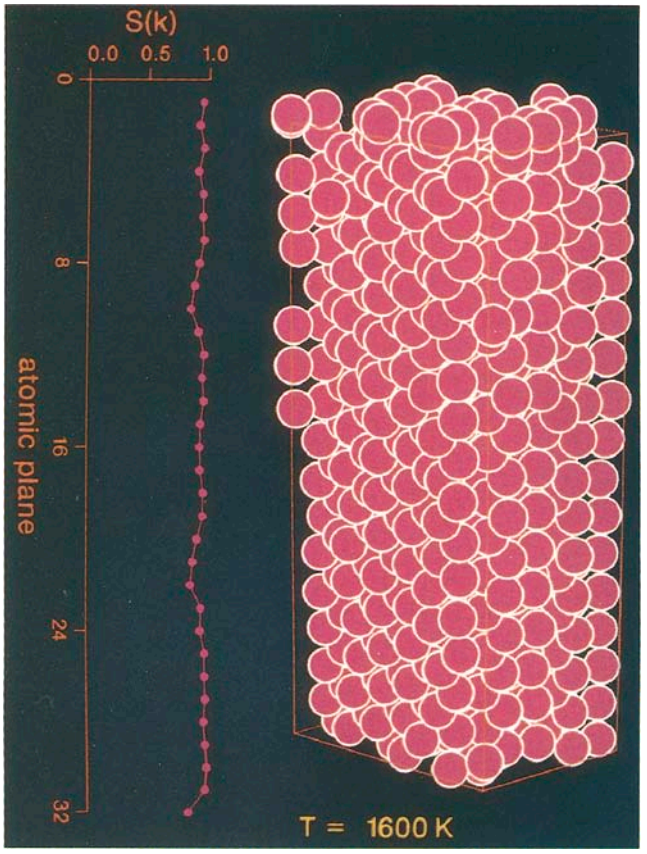

Fig.3: Ideal-crystal computational cell of 704 atoms, stacked in 32 (110) planes, each containing 22 Si atoms. The limits of the cell are indicated by the gold box, beyond which 3-d periodic border conditions are applied to simulate an infinitely large perfect crystal. After gradually heating to 1600K (i.e., 91K below T_m for the Stillinger-Weber potential), all atoms have the ideal-crystal coordination of four. Here and in subsequent figures, the color of atoms indicates their nearest-neighbor coordination K, with red, blue and green denoting, respectively, $K = 4$, $K \leqslant 3$ and $K \geqslant 5$.

The plane-by-plane profile of the order parameter, $S(k)$, at 1600K is shown on the left for a reciprocal lattice vector, $\mathbf{k}$, in the $<110>$ direction within each of the (110) planes (see Eq. (3)). The values of $S(k)$ near unity illustrate the large degree of crystalline long-range ordering within the (110) planes, in spite of the substantial thermal vibrations of the atoms at this very high temperature.

$S_p(\mathbf{k})$, the square of which represents the desired order parameter, according to

$$\xi \equiv [S_p(\mathbf{k})]^2 = [1/N \Sigma_{i(p)} \cos(\mathbf{k}\cdot\mathbf{r}_i)]^2 + [1/N\Sigma_{i(p)} \sin(\mathbf{k}\cdot\mathbf{r}_i)]^2, \quad (3)$$

in which only atoms $i = i(p)$ in a given lattice plane, p, are considered. (As discussed below, in all of our simulations p will vary within the range $1 \leqslant p \leqslant 32$.) For a perfect crystal lattice at zero temperature, ξ is identically equal to one for any wave vector, $\mathbf{k}$, which is a reciprocal lattice vector in that plane. By contrast, in the liquid state,

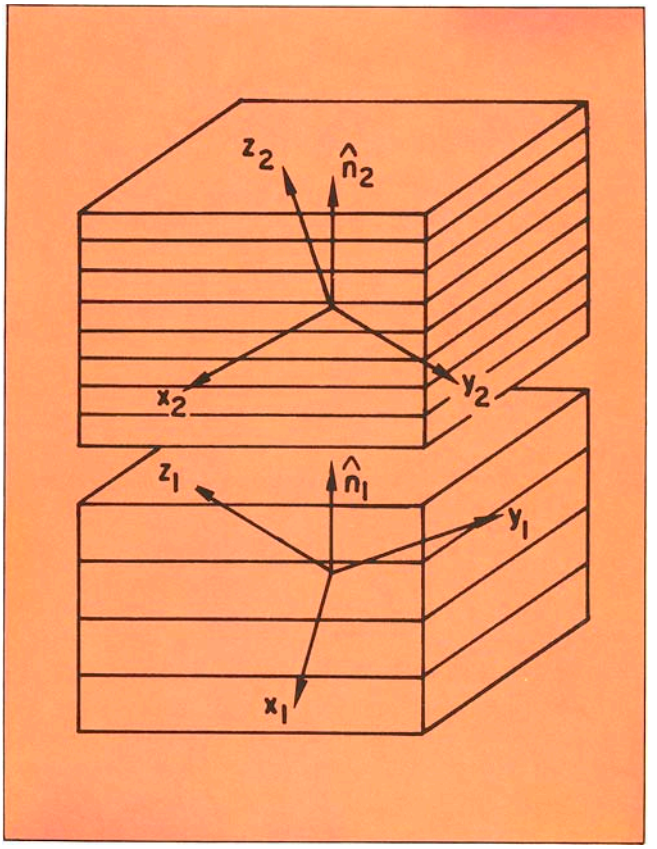

Fig.4: Definition of the five degrees of freedom of a general grain boundary contained in a bicrystal. Far from the boundary plane in the direction of the interface-plane normal, the inhomogeneous region containing the interface is on both sides embedded between perfect-crystal material.

---

without any long-range order in the planes, ξ fluctuates near zero. As a reminder of its association with the static structure factor, in the following the order parameter will be denoted simply by $S(k)$ ($\equiv \xi$).

When the crystal is heated from absolute zero, the value of $S(k)$ is reduced slightly from unity because of the lattice vibrations. This effect is illustrated in Fig.3 for a crystal containing a total of 704 Si atoms (arranged in 32 (110) planes, each of which contains 22 atoms in the rectangular planar unit cell; the reason for the choice of this particular unit cell will become more apparent below). In this simulation, as is common in MD simulations, three-dimensional (3-d) periodic border conditions were applied to the simulation cell in order to approximate an infinitely large crystal. The crystal shown in Fig.3 was slowly heated from zero temperature to 1600K, which is 91K below the thermodynamic melting point for the Stillinger-Weber potential. At this temperature all atoms are perfectly coordinated, with four nearest neighbors. The plane-by-plane order parameter, shown in the left of the figure, demonstrates a typical reduction by about 10 percent at this elevated temperature due to the lattice vibrations. The reduction in $S(k)$ from unity is governed by the so-called Debye-Waller factor which represents a measure for the average vibrational amplitude of the atoms at a given temperature.

Role of Grain Boundaries

Grain boundaries are of considerable interest in the context of melting because most real materials are polycrystals. A grain boundary is generally characterized by five geometrical degrees of freedom (DOF) defined in Fig.4, which illustrates the formation of a bicrystal, with the grain boundary (GB) in its center, by joining two single crystals along two well-defined crystallographic planes. We recall that any crystallographic direction, $\hat{n}$, given for example in terms of Miller indices, $<h,k,l>$, represents *two* DOF, according to

$$\hat{n} = (h^2 + k^2 + l^2)^{-1/2} \begin{pmatrix} h \\ k \\ l \end{pmatrix}. \qquad (4)$$

As illustrated in Fig.4, the characterization of the 5 DOF of the grain boundary starts with defining the GB-plane normal, $\hat{n}$, in each of the two principal coordinate systems, (x_1, y_1, z_1) and (x_2, y_2, z_2), associated with the two halves of the bicrystal. For example, the GB-plane normal $\hat{n}_1$ in the first of the two semicrystals might be a $<110>$ direction while in the other crystal the normal, $\hat{n}_2$, might be a $<111>$ direction.
With the GB-plane normal thus fixed with respect to the two crystals (and thus having defined four of the 5 DOF), the only remaining DOF is the one associated with a so-called twist rotation about $\hat{n}$, characterized by the twist angle θ (see Fig.4). The 5 DOF of a general grain boundary may then be summarized as follows:

$$\{\text{DOF}\} = \{\hat{n}_1,\ \hat{n}_2,\ \theta\}. \qquad (5)$$

In a symmetrical grain boundary, $\hat{n}_1$ and $\hat{n}_2$ represent the same set of crystallographically equivalent lattice planes (i.e., $\hat{n}_1 = \hat{n}_2$), leaving only three DOF, namely $\hat{n}$ and θ.

The GB we have studied is symmetrical, with the GB plane being a (110) plane. To introduce the GB into the bicrystal, the one half is rotated by $\theta = 50.48°$ with respect to the other about the $<110>$ plane normal. In terms of Eq.(5) this interface is therefore characterized by $\{\text{DOF}\} = \{<110>, <110>,\ 50.48°\}$. In the jargon of the grain-boundary community, this boundary is referred to as the (110) 50.48° (Σ11) twist boundary. The value of Σ indicates that the area of its planar unit cell is $\Sigma = 11$ times larger than that of a perfect-crystal (110) plane in Si (see Figs.1 and 2). The unit-cell dimensions of this GB, illustrated in Fig.5, explain our earlier choice of simulation cells for the perfect-crystal simulation: this choice renders the simulation-cell dimensions identical for the perfect crystal, the thin slab and the bicrystal, the only difference arising from the different border conditions imposed on this cell.

Similar to Fig.3, each of the 32 (110) planes in the bicrystal contains 22 atoms. With an interplanar spacing of (110) planes in Si of $d(110) = 0.354a$, the length of the computational cell is 11.33a. The planar unit-cell area of $2.345a \times 3.317a = 7.778a^2$ is 11 times that of the corresponding primitive planar unit cell indicated in Fig.1. (Notice that the planar dimensions in both the primitive and the simulation cell are related by $\sqrt{2}$.) The computational cell thus contains 704 Si atoms in a volume of $88.129a^3$.

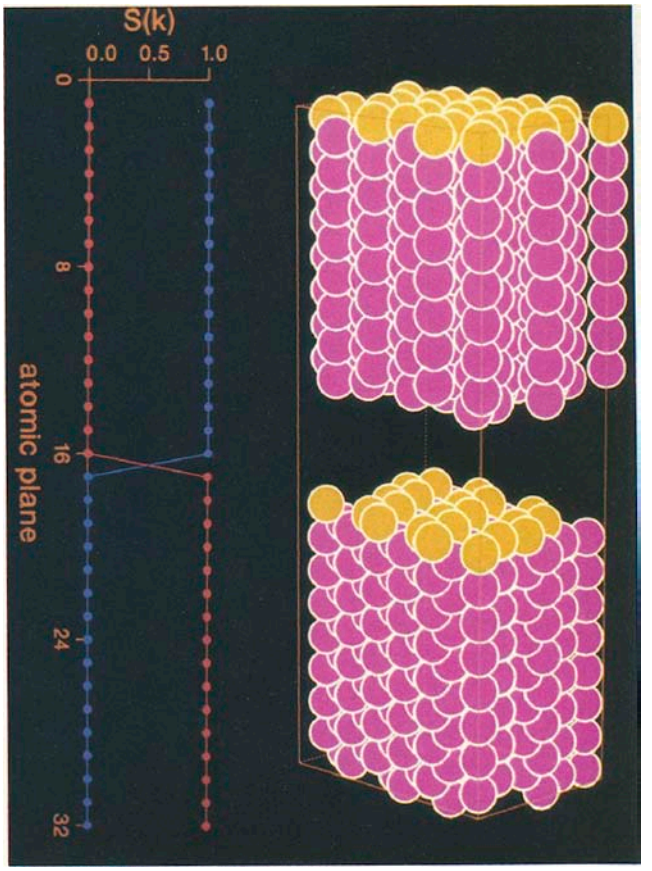

Fig.5: $(110)\theta = 50.48°$ bicrystal of Si at zero temperature. The bottom half of the bicrystal has the same orientation as the computational cell used in the perfect-crystal and thin-slab simulations (see Figs. 3 and 8). The upper half of the bicrystal is rotated by $\theta = 50.48°$ about the $<110>$ common grain-boundary plane normal. The atoms in the top plane of each half of the bicrystal are colored in yellow to highlight their relative rotation. For illustrative purposes, in this and in the following figure, the top and bottom halves of the bicrystal are separated, so as to make the evolution of the system more clear. As discussed in the text, the two wave vectors, $\mathbf{k}_1$ and $\mathbf{k}_2$, in the order parameters $S(\mathbf{k}_1)$ and $S(\mathbf{k}_2)$ (indicated, respectively, in red and blue in the left of the figure) represent reciprocal planar lattice vectors in the related half of the bicrystal. At zero temperature, in semicrystal 1 we then have, $S(\mathbf{k}_1) = 1$ and $S(\mathbf{k}_2) = 0$ whereas in semicrystal 2, $S(\mathbf{k}_2) = 1$ and $S(\mathbf{k}_1) = 0$.

Far from the interface, which is characterized by a 2-d periodic arrangement of atoms parallel to the GB plane, any grain boundary is surrounded by perfect-crystal material. As in the thin-film simulations discussed later, we apply 2-d periodic border conditions in the interface plane to simulate the infinite size of the bicrystal parallel to the GB plane. However, in the direction of the GB-plane normal neither the free borders of the thin film nor the periodic borders of the perfect crystal are appropriate. By surrounding the simulation cell on both sides of the grain boundary with rigid perfect-crystal blocks which are allowed to slide parallel and perpendicular to the interface

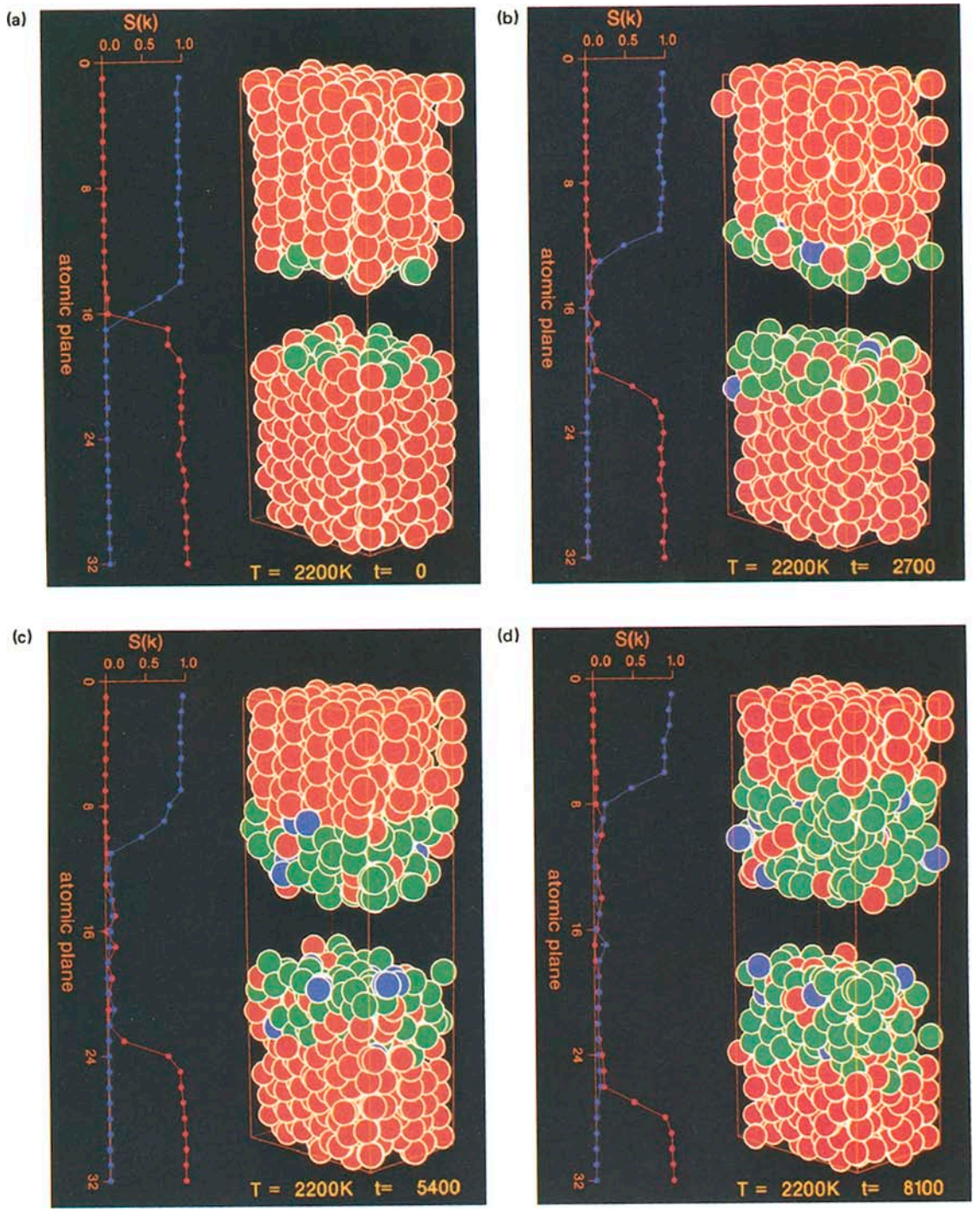

Fig.6: Heterogeneous "thermodynamic melting" of a silicon bicrystal containing in its center the (110) $\theta = 50.48°$ ($\Sigma 11$) grain boundary. After having been heated over a period of 600 time steps from 1600K ($T < T_m$) to 2200K ($T > T_m$), the time was reset to $t = 0$. 1000 time steps corresponds to 1.15 psec of real time. The color of the atoms indicates their nearest neighbor coordination K, with red, blue and green denoting, respectively, $K = 4$, $K \leqslant 3$ and $K \geqslant 5$.
(a) At $t = 0$ (i.e., immediately after the simulation temperature of 2200K was reached), there are a number of atoms at the grain boundary that already have coordination greater than four. The order parameters show, however, the sharp definition of the GB region containing only about 4 (110) planes.
(b) After 2700 time steps, a number of planes on either side of the GB plane have melted. The near-zero values of the structure factor show that long-range order has now broken down in approximately seven (110) planes closest to the GB.
(c) After 5400 time steps more planes have melted.
(d) After 8100 time steps over half of the system has melted; long-range order has been lost in the 20 central planes of the system.

plane, thus enabling both GB migration and a volume expansion at the boundary, we have recently developed a border condition which permits a realistic simulation of "bulk" interfaces, i.e., interfaces embedded between perfect material.

In contrast to the perfect-crystal, *two* order parameters are now required to investigate the breakdown of planar crystalline order upon melting, one associated with each half of the bicrystal. By choosing two wave vectors, $\mathbf{k}_1$ and $\mathbf{k}_2$, which are reciprocal lattice vectors in the (110) planes associated with the two semicrystals, we define the order parameters $S(\mathbf{k}_1)$ and $S(\mathbf{k}_2)$ in analogy to Eq.(3). ($\mathbf{k}_1$ and $\mathbf{k}_2$ are thus simply related by the relative rotation of the two halves of the bicrystal about the $<110>$ GB-plane normal.) By monitoring these two order parameters, every lattice plane may then be characterized as either being totally disordered (for $S(\mathbf{k}_1)\approx S(\mathbf{k}_2)\approx 0$), as belonging to semicrystal 1 (for $S(\mathbf{k}_1)\approx 1$, $S(\mathbf{k}_2)\approx 0$), or as belonging to semicrystal 2 (for $S(\mathbf{k}_2)\approx 1$, $S(\mathbf{k}_1)\approx 0$). A slice-by-slice order-parameter profile (illustrated in Fig.5 for zero temperature) then shows a sudden drop at the GB in $S(\mathbf{k}_1)$ from unity to zero (red symbols in the left of Fig.5), while $S(\mathbf{k}_2)$ increases simultaneously from zero to one (blue symbols).

To investigate the high-temperature behavior of the bicrystal, the system was first equilibrated at 1600K. The temperature was then stepped up rather rapidly in intervals of 100K, allowing 100 time steps for approximate equilibration, until the desired final simulation temperature, ranging between 1800K and 2200K, was reached; this instant will be labeled $t = 0$. As already mentioned, the average atomic coordination increases from four to approximately six upon melting. To illustrate the different local environments of the atoms in the bulk, a surface or in the liquid, throughout our discussion red atoms will indicate perfect-crystal coordination ($K = 4$), with green atoms indicating $K > 4$ while for blue atoms $K < 4$.

The response of the bicrystal when heated to a temperature above T_m is shown in the four snapshots in Fig.6, which is characteristic of all of our grain-boundary simulations. It appears that melting begins at the grain boundary, from which the melted layer then spreads into the bulk regions. The snapshot at $t = 0$ (i.e., immediately after reaching the desired simulation temperature) illustrates two important features. First, as indicated by the absence of blue atoms, all Si atoms near the GB are at least four-fold coordinated. The presence of a significant number of green atoms suggests that numerous atoms near the GB have already reached liquid-like coordination during the short heating period above T_m. Second, as demonstrated by the crossing of $S(\mathbf{k}_1)$ and $S(\mathbf{k}_2)$ in the left of Fig.6, and by the narrow region of only about four (110) planes in which the order parameters deviate significantly from unity, the GB is sharply defined, as sharply as it was prior to raising the temperature from 1600K to a temperature above T_m.

The order parameters in the left of Figs.6(b)-(d) clearly show the propagation of two interfaces which separate areas of well-ordered (110) planes from areas with no planar long-range order at all (and, consequently, with S(k) fluctuating near zero). A detailed analysis of

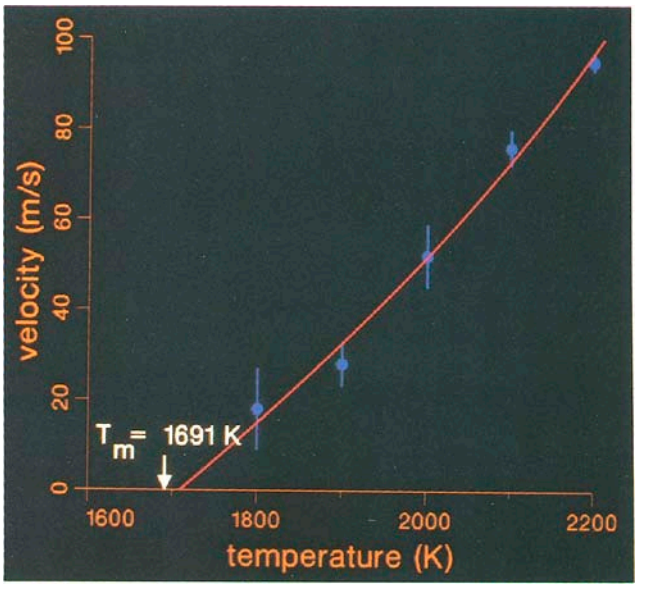

Fig.7: Propagation velocities of the solid-liquid interfaces as a function of temperature. The red curve, representing a quadratic fit to the data points, extrapolates to zero velocity at $T = 1710 \pm 30$K, as compared with the thermodynamic melting temperature of the Stillinger-Weber potential of $T_m = 1691 \pm 20$K.

the atom positions in the direction of the GB-plane normal shows the breakdown of a planar atom arrangement in the regions with vanishing order parameter. That the disordered region is, indeed, *liquid* (and not merely disordered like in an amorphous solid) was verified in two ways. First, the related volume contraction upon melting agrees well with that determined from an independent simulation of liquid silicon. Second, the plane-by-plane mean-square displacements, $<r^2>$, of the atoms are found to increase linearly with simulation time in the disordered regions, but to be practically constant in the crystalline regions away from the GB. In MD simulations, such a linear increase in $<r^2>$, associated with the random walk of the atoms during self-diffusion, is considered a fingerprint of a liquid. Moreover, the value of the self-diffusion constant extracted from the slope of $<r^2>$ versus t is in good agreement with that determined from separate simulations of the liquid at the same temperature. We therefore conclude that the disordered regions are, indeed, liquid.

The above simulations reveal that melting begins at the grain boundary from which the liquid phase penetrates into the crystalline region via the propagation of two solid-liquid interfaces. To actually follow the movement of these interfaces requires a certain amount of data analysis because the atoms move continuously, and the position of the interface is not always easy to determine. Nevertheless, from the results of our simulations at several temperatures above T_m, propagation velocities for the spreading of the solid-liquid interfaces into the crystalline regions, v, can be extracted. In Fig.7 these velocities are plotted as function of temperature. Extrapolation of these temperature-dependent velocities to zero velocity should yield an estimate of the coexistence temperature, T_m, at

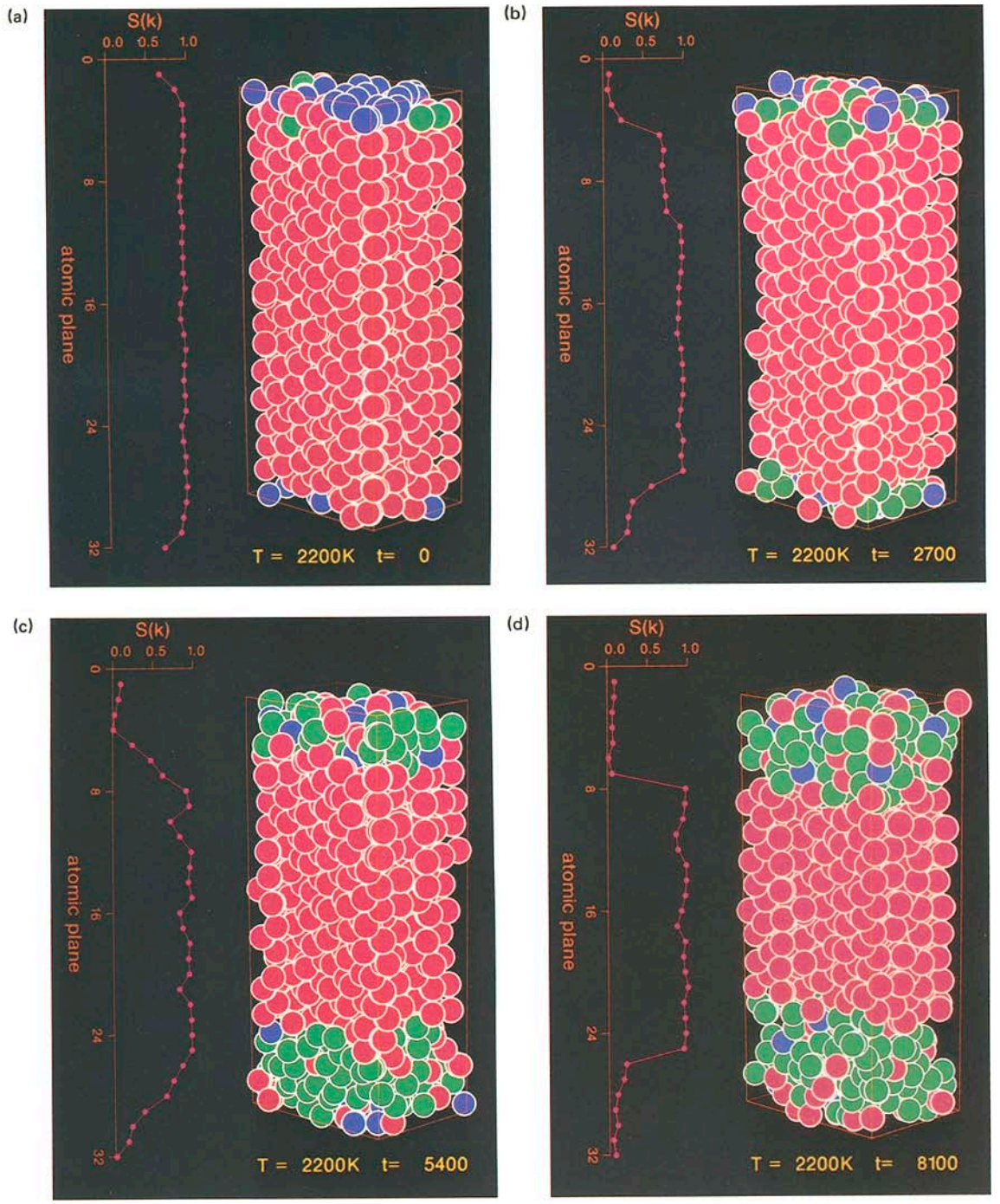

Fig.8: Evolution with time of a thin slab with (110) faces after having been heated over a period of 600 time steps from 1600K ($T < T_m$) to 2200K ($T > T_m$), at which instant the time was reset to $t = 0$. 1000 time steps correspond to 1.15 psec of real time. The color of the atoms indicates their nearest-neighbor coordination K, with red, blue and green denoting, respectively, $K = 4$, $K \leqslant 3$ and $K \geqslant 5$.

(a) At $t = 0$ most atoms on the surfaces are three-fold coordinated (blue balls), due to the removal of one nearest neighbor on creation of the free surface. A few surface atoms have already become greater than four-fold coordinated during the 500 time steps during which the system was at $T > T_m$.

(b) After 2700 time steps more atoms are liquid-like coordinated (green balls), although the liquid region has hardly spread into the bulk. Note however, that the structure factor shows the breakdown of in-plane long-range order for a number of planes away from the surfaces.

(c) After 5400 time steps there are significant regions of melted material near the two free surfaces. As indicated in the order parameter, a thermal fluctuation has apparently caused a small amount of recovery in the long-range order of the system near the lower free surface.

(d) After 8100 time steps approximately half the system has melted, as indicated by the near-zero values of the order parameter for a number of planes near each of the two free surfaces.

which the crystal and liquid are in thermodynamic equilibrium, and at which, therefore, the solid-liquid interface will not propagate. The temperature so obtained from Fig.7 is 1710 ± 30K, in remarkable agreement with the temperature of 1691 ± 20K obtained from the free-energy analysis of Broughton and Li.

We conclude from the above evidence that above T_m the grain boundary nucleates the liquid phase which subsequently grows into the crystal, a process requiring thermally-activated diffusion kinetics.

Effect of Free Surfaces

Rather than investigating a single isolated free surface attached to a practically infinite bulk perfect crystal underneath, we consider a thin slab, consisting of 32 (110) planes of atoms, with the outermost planes representing free surfaces. The initial separation between the surfaces (i.e. without atomic relaxations nor thermal expansion) is 11.33a. This film thickness was found to be large enough to ensure that the two surfaces do not interact noticeably over the duration of the simulation (10,000 time steps $\approx$ 11 ps). In contrast to the simulation of the defect-free perfect crystal and the bicrystal, the border conditions imposed on the simulation cell are now chosen to be periodic only in the two dimensions parallel to the free surfaces, with the latter surrounded by vacuum.

The thin film was heated to 2200K using the same procedure as that used in the grain-boundary studies. Figure 8, characteristic for all of our thin-film simulations, shows four snapshots of the system starting immediately after the desired simulation temperature of 2200K was reached. The snapshot at $t = 0$ illustrates the relatively poor coordination of the atoms in the free surface (blue atoms), in contrast to the perfectly coordinated atoms in the interior region of the slab. The order parameter in the left of the figure, well above 0.5 throughout the simulation cell, indicates a well-ordered planar arrangement of the atoms. The smaller values at the two surfaces are primarily due to the larger vibrational amplitudes of the surface atoms.

The following snapshots after 2700, 5400, and 8100 time steps demonstrate the rapid increase in the number of atoms with coordination in excess of four, suggesting that the surface regions have actually melted. As in our grain-boundary simulations, we have verified that the atoms are, indeed, in the liquid state by determining the diffusion coefficient in the disordered region. The spreading velocities extracted from these simulations are statistically identical to those obtained from the analysis of the grain-boundary simulations.

One might ask whether other extended defects can also act as nucleation centers. This question was investigated in a similar melting study for the face-centered cubic metal copper. In this work we considered the effect of voids of various sizes, with the main conclusion that a void is, indeed, able to nucleate the liquid provided it is large enough and relatively immobile.

From the above evidence, we conclude that above T_m grain boundaries, free surfaces or voids (and we may reasonably expect, lattice dislocations as well) can nucleate the liquid phase which subsequently grows into the crystal—a process requiring thermally-activated diffusion kinetics. Melting is therefore a relatively slow heterogeneous process nucleated at internal or external surfaces. The propagation velocities in Fig.7, typically of the order of a few dozen m/s, are of the same order of magnitude as the velocities obtained from laser-annealing experiments on Si. Given a value, say, of 100m/s, obtained at $\sim$500K above the melting point (see Fig.7), a single crystal 1cm in diameter would require approximately 50μs to melt. This value indicates that melting is by no means an instantaneous process. Also, since our simulation cells contained no *intrinsic* lattice defects, the above simulations question the validity of theories of melting based on the presence of such defects.

Melting of a Defect-Free Crystal

In computer simulations, thermodynamic melting is easily suppressed by elimination of extended defects, for example, via the application of 3-d periodic border conditions to the perfect-crystal simulation cell in Fig.3. Experimentally, due to the presence of free surfaces and, in most materials, a sufficient atomic concentration of lattice dislocations, superheating is extremely difficult to achieve as discussed earlier.

Over half a century ago Born pointed out the existence of an absolute limit to superheating of any crystalline substance. By considering the volume dependence of the normal modes of a crystal lattice, he demonstrated the existence of a phonon instability at a certain critical volume of the system. By couching the discussion in terms of the elastic constants (which are known to be intimately connected with the long-wavelength lattice vibrations), Born's phonon instability can be shown to correspond to an elastic instability in the shear constant C_{44} which, for a crystal lattice with cubic symmetry and in the proper coordinate system, is given by $(C_{11}-C_{12})/2$. This instability, occurring when C_{11} and C_{12} become equal, signifies no resistance of the crystal lattice to certain shear strains.

The physical meaning of Born's limit becomes particularly apparent when we consider the Poisson ratio, ν, which together with Young's and the shear modulus is needed to characterize the elastic performance of engineering materials. When a tensile strain, $\varepsilon = \Delta l/l$, is imposed on a tetragonal prism of length l and square lateral dimensions d, the consequent contraction, $\Delta d/d$, perpendicular to the direction of the applied stress is governed by the Poisson ratio, defined by

$$\nu = (\Delta d/d) \;/\; (\Delta l/l) \qquad (6)$$

Because the imposed strain is tensile, the resulting volume change of the prism,

$$\Delta V/V = [(d-\Delta d)^2 (l + \Delta l) - d^2 l]/d^2 l \sim \varepsilon\,(1-2\nu) \qquad (7)$$

has to be positive, i.e., $0 \leqslant \nu \leqslant 0.5$. For a single crystal with cubic symmetry, ν may be expressed in terms of C_{11} and C_{12} as follows:

$$\nu = C_{12} \;/\; (C_{11} + C_{12}) \qquad (8)$$

The condition that $\nu \leqslant 0.5$ therefore requires that C_{12} cannot exceed C_{11}. At the instability point, at which

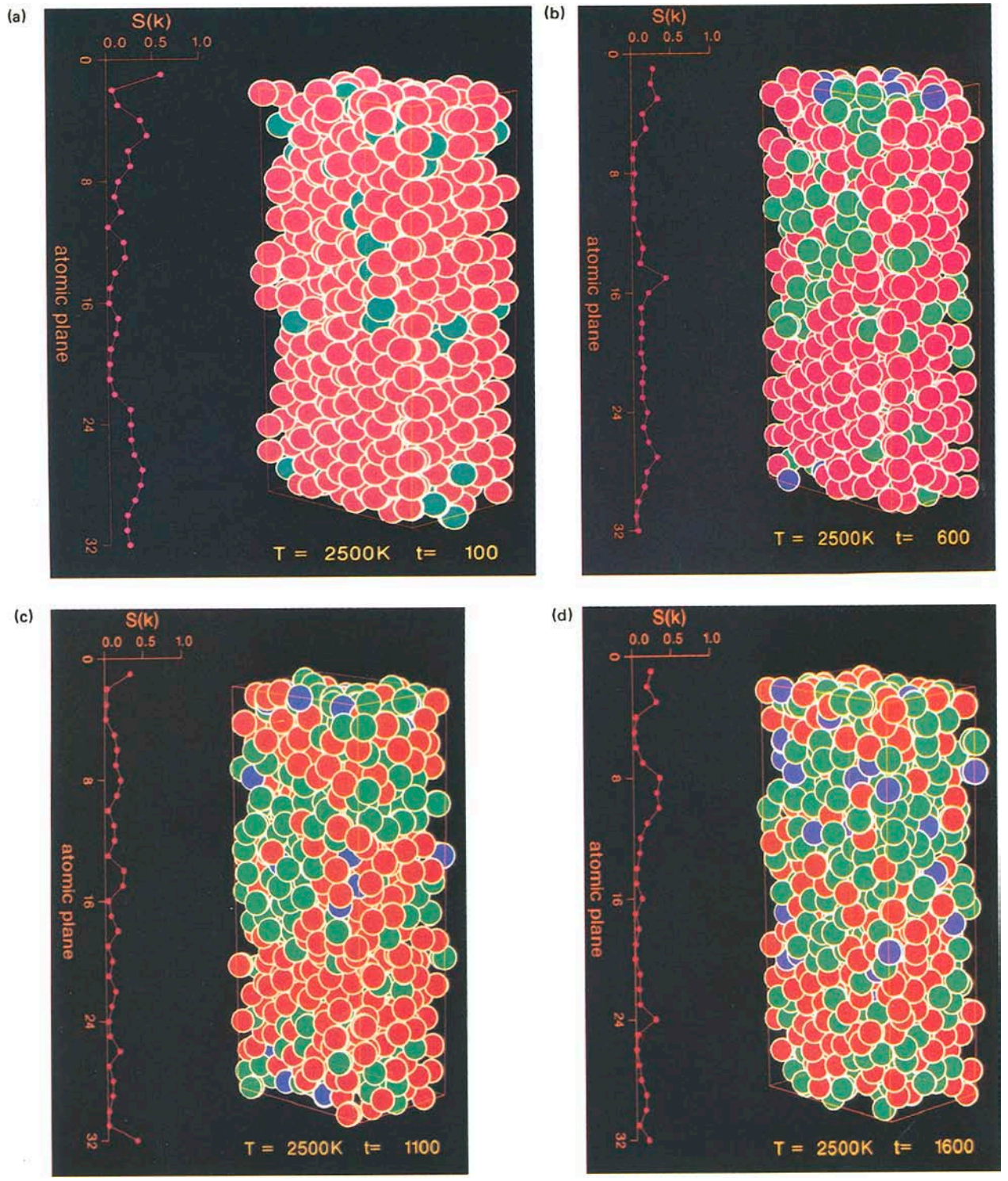

Fig. 9: Homogeneous "mechanical melting" of the defect-free perfect crystal of Fig. 3, realized via application of 3-d periodic border conditions. Although the unit-cell dimensions are identical to those of the bicrystal in Fig. 4 and of the thin slab in Fig. 8, the 3-d periodic border conditions produce effectively an infinitely large perfect crystal. A comparison with Figs. 6 and 8 demonstrates how rapidly the process of mechanical melting takes place by comparison with the thermodynamic melting mechanism. Figs. 9(a)-(d) also demonstrate that the process occurs *homogeneously*, in contrast to the nucleation-and-growth controlled mechanism of thermodynamic melting.

(a) Only 100 time steps after reaching the simulation temperature, a number of defected, i.e., not perfectly coordinated atoms is found to be scattered randomly throughout the system. Note that the long-range order has practically broken down already throughout the entire crystal, as evidenced by the near-zero values of the related order parameter, S(**k**), in the left of the figure.

(b)-(d) After 600, 1100, and 1600 time steps, respectively, more and more liquid-like coordinated atoms are found in the simulation cell, and the order parameter fluctuates near zero.

$C_{11} = C_{12}$ (and therefore $\nu > 0.5$), the volume of the crystal would actually *decrease* under tension (rather than increase).

Given that, due to anharmonic effects, virtually all materials expand upon heating, Born's criterion establishes the existence of a maximum volume expansion of a superheated crystal lattice, coupled with a maximum superheating temperature, above which the crystal is mechanically unstable and therefore has to undergo some kind of phase transformation (into the liquid state or into some other crystal structure). The temperature associated with the maximum superheating limit under zero external pressure (thus including the effects of thermal expansion), is referred to as the mechanical melting point, T_s, to be distinguished from the thermodynamic melting temperature, T_m. (The subscript "s" refers to "stability".)

In our simulations of metals, the evaluation of C_{11} and C_{12} gives typical values of T_s about 20% above T_m. By contrast, we estimate T_s in Si to exceed T_m by as much as 40% (i.e., $T_s \sim 2500$K). In practice it is very difficult, even in simulations, to reach T_s because of statistical fluctuations in the volume and temperature of the system. By gradually stepping up the temperature, we were able to superheat a perfect Si crystal to 2400K, i.e., 700K above T_m; beyond this temperature the crystal could not be stabilized.

Analogous to the free-energy calculation which predicts T_m, the determination of T_s does not provide information on the *mechanism* by which the crystalline order breaks down. To investigate this mechanism, we have simulated the melting of a defect-free crystal. Figs.9(a)-(d) illustrate how rapidly the perfect crystal melts above T_s. After a step increase of the simulation temperature from below T_s to 2500 K, only a few hundred MD time steps (i.e., only a few lattice-vibration periods) are required to completely destroy the long-range order within the (110) planes. Moreover, the order-parameter profiles in Figs.9(a)-(d) show that planar order is lost simultaneously in all parts of the crystal. This evidence suggests that the liquid phase is formed *homogeneously*.

The above simulation shows clearly the phenomenon of superheating. The reason that it is so easily visible by simulation, in contrast to experiments, is due to the fact that, via the application of 3-d periodic border conditions, surfaces are easily eliminated entirely from the simulation cell.

Characteristics of Thermodynamic and Mechanical Melting

The above simulations illustrate that every crystal, in principle, has two melting points, T_m and T_s. Conceptually the two transitions have distinct physical origins: while *thermodynamic melting* is governed by the free energies of the liquid and the solid phases, *mechanical melting* is based on a phonon instability. Since at ambient pressure, the volume expansion required for mechanical melting is always larger than that associated with thermodynamic melting, the free energy always favors thermodynamic over mechanical melting; i.e., $T_s > T_m$. However, as illustrated above, the former requires atomic mobility, and may therefore be kinetically hindered. If a crystal is melted under atmospheric conditions, the thermodynamic state variables usually will be such that high atom mobility in the liquid enables the nucleation and growth of the liquid phase at extended defects. However, if for example by uniformly expanding the crystal, melting is induced at a lower temperature, the consideration of limited atom mobility as a possible hindrance to phase change may be of significant importance. The crystal may, indeed, not be able to disorder at the volume specified by equilibrium thermodynamics until a larger volume is reached where the mechanical instability can occur.

There is considerable experimental evidence that solid-state amorphization, the process in which the long-range crystalline order is destroyed by external means (such as mechanical or chemical means, or by irradiation), can proceed by the same two distinct mechanisms as melting and that, in contrast to conventional melting, both types of transition can actually be observed. In a typical melting experiment, the order-disorder transition is induced by increasing the temperature (T) under ambient pressure (P), thus allowing the volume (V) to expand, a procedure guaranteeing high atom mobility at the point (T, P(V)) in thermodynamic phase space where the transition can occur. In a typical solid-state amorphization experiment, by contrast, the temperature is held fixed at some relatively low value, well below T_m. The role of the irradiation, or of the mechanical or chemical means, in inducing the crystal-to-amorphous transition is to expand the crystal lattice to the coexistence point in phase space where the thermodynamic transition can, in principle, occur. However, relatively low atom mobility gives rise to a competition between the heterogeneous and homogeneous processes, a competition governed by the level of atomic mobility at that point in phase space. Hence, while at higher temperatures mechanical amorphization will be preempted by the thermodynamic type of transition, at lower temperatures this type of transition may be kinetically hindered due to the reduced atom mobility. However, at an even larger volume expansion than that at the thermodynamic coexistence point at a fixed temperature, the ultimate stability limit of the crystal may be reached, thus enabling a fast, homogeneous transition into the liquid state. Due to the low atomic mobility this non-crystalline state appears to be solid, although it merely represents a kinetically arrested liquid.

Let us summarize the three main distinguishing characteristics of thermodynamic and mechanical melting.

(a) Whereas thermodynamic melting is based on the *free energies* of both the crystalline and liquid states, mechanical melting is triggered by a *phonon instability*.

(b) Thermodynamic melting is a *heterogeneous* process, involving nucleation and growth of the liquid phase at extended defects, whereas mechanical melting takes place *homogeneously*, without the need for the presence of lattice defects.

(c) The growth of the liquid phase into the crystal (by propagation of solid-liquid interfaces) requires thermally-activated *diffusion kinetics* in the liquid. Mechanical melting, by contrast, takes place typically within a few lattice vibration periods independent of temperature.

In concluding we point out that, in our view, the present study provides an illustration of several unique features of atomistic simulation, namely the abilities to prescribe precisely the initial system configuration, to control the dynamic environment during the simulations, and to follow the system response in complete detail, all at the atomic level. It seems clear that in future simulation studies of complex physical phenomena these capabilities will be explored to an even greater extent. In doing so one should keep in mind that the significance of the simulation results is always limited by the reality of the interatomic potential function used. For this reason one should look for *insight* from simulation rather than merely numerical results.

Acknowledgments: We gratefully acknowledge access to the Energy Research computing facility at the Magnetic Fusion Computational Center at Livermore, CA, and to the facilities of the Electron Microscopy Center at Argonne and the support of N. J. Zaluzec. This work was supported by the U.S. Department of Energy, BES Materials Sciences, under Contract W-31-109-Eng-38.

FOR FURTHER READING

J. Q. Broughton and X. P. Li, *Phase Diagram of Silicon by Molecular Dynamics*, Physical Review B**35**, 1987, p.9120.

R. L. Cormia, J. D. Mackenzie and D. Turnbull, *Kinetics of Melting and Crystallization of Phosphorous Pentoxide*, Journal of Applied Physics **34**, 1963, p.2239.

R. W. Cahn and W. L. Johnson, *The Nucleation of Disorder*, Journal of Materials Research **1**, 1986, p. 724.; see also R. W. Cahn, *Melting and the Surface*, Nature **323**, 1986, p.668.

J. F. Lutsko, D. Wolf, S. Yip, S.R. Phillpot and T. Nguyen, *Molecular-Dynamics Method for the Simulation of Bulk Solid Interfaces at High Temperature*, Physical Review B**38**, 1988, p.11 572.

S. R. Phillpot, J. F. Lutsko, D. Wolf and S. Yip, *Molecular-Dynamics Study of Lattice-Defect Nucleated Melting in Silicon*, Physical Review B**40**, 1989, p.2831, and *Molecular-Dynamics Study of Lattice-Defect Nucleated Melting in Metals using an Embedded-Atom-Method Potential*, ibid., p.2841.

A. R. Ubbelohde, *Molten State of Matter: Melting and Crystal Structure*, Wiley, Chichester, 1978.

D. Wolf, P. R. Okamoto, S. Yip, J.F. Lutsko, and M. D. Kluge, *Thermodynamic Parallels Between Solid-State Amorphization and Melting*, Journal of Materials Research, Nov./Dec.1989 (in press).